ISSN 1027-5495. Functional Materials, 33, No.3 (2026), p. 573-582
doi:http://dx.doi.org/10.15407/fm33.03.573 © 2026 — SSI "Institute for Single Crystals"
This is an open access article under the CC BY-NC-ND license (http://creativecommons.org/licenses/by-nc-nd/4.0/).

3D printing by direct ink writing of heater prototypes for ceramic fuel cells from mechanosynthesized $MoSi_2$ nanopowder

I. Poliakov, V. Naumenko*, I. Kud, R. Mediukh, O. Myslyvchenko, Ye. Brodnikovskyi, O. Zgalat-Lozynskyy

Frantsevich Institute for Problems of Materials Science NAS of Ukraine
Corresponding author e-mail: v.naumenko@ipms.kyiv.ua

Received July 27, 2026, approved August 25, 2026

This study presents a comprehensive investigation of the mechanosynthesis of molybdenum disilicide ($MoSi_2$) nanopowder and its subsequent application in the fabrication of ceramic heating elements for stacks of solid oxide fuel cells (SOFCs). SOFCs are a promising technology for stationary energy generation due to their high efficiency in converting chemical energy into electricity (up to 65%) and heat (up to 30%), fuel flexibility (hydrogen, hydrocarbons, CO, etc.), and absence of platinum-group catalysts. $MoSi_2$ was selected as a material for heating elements due to its high electrical and thermal conductivity, exceptional thermal stability, resistance to oxidation, and ability to withstand high operating temperatures, making it suitable for rapid and uniform heating in SOFC stacks. The influence of the powder-to-ball mass ratio (1:10 and 1:20) and milling parameters on the mechanosynthesis process was systematically studied. It was found that higher energy input significantly accelerates the formation of the $MoSi_2$ phase, reducing the reaction time by approximately 1.5 times. X-ray diffraction analysis confirmed the formation of the $MoSi_2$ phase with minor residual molybdenum, while silicon was found to be X-ray amorphous, indicating its high reactivity and structural disorder after mechanical activation. Energy transfer during milling and particle size distribution were analyzed to optimize synthesis parameters, ensuring uniform nanopowder morphology suitable for further processing. The synthesized nanopowder was used to prepare ceramic pastes for 3D printing via the robocasting method. The rheological properties of the pastes were optimized to allow stable extrusion and high-resolution printing of complex geometries. Key printing parameters, including extrusion rate, nozzle diameter, and printing speed, were adjusted to minimize defects and ensure the structural integrity of printed elements. After thermal treatment and sintering, the printed heating elements exhibited rapid and uniform temperature rise, demonstrating their suitability for integration into SOFC stacks and other high-temperature energy-generating systems.This work provides a detailed methodology for combining mechanosynthesis and additive manufacturing to produce high-performance ceramic components. The results contribute to the development of energy-efficient and reliable heating elements for advanced SOFCs and demonstrate the potential of $MoSi_2$-based materials in high-temperature energy applications. Furthermore, the findings offer insights into controlling phase composition, particle morphology, and process parameters, which are critical for the scalable production of functional nanostructured ceramics.

Keywords: mechanosynthesis, $MoSi_2$, additive technologies, DIW, solid oxide fuel cells, 3D printing.

3D друк методом прямого друку чорнилами прототипів нагрівачів для керамічних паливних комірок з механосинтезованого нанопорошку $MoSi_2$.
І.А. Поляков, В.Ю. Науменко, І.В. Кудь, Р.М. Медюх, О.М. Мисливченко, Є.М. Бродніковський, О.Б. Згалат-Лозинський

У роботі представлено комплексне дослідження механосинтезу нанопорошку дисиліциду молібдену ($MoSi_2$) та його подальше використання для виготовлення керамічних нагрівальних елементів для стеків твердотільних оксидних паливних комірок (SOFC). SOFC є перспективною технологією для стаціонарної генерації енергії завдяки високій ефективності перетворення хімічної енергії в електричну (до 65%) та теплову (до 30%), гнучкості щодо вибору палива (водень, вуглеводні, CO тощо) та відсутності каталізаторів платинової групи. $MoSi_2$ було обрано як матеріал для нагрівальних елементів завдяки його високій електро- та теплопровідності, винятковій термічній стабільності, стійкості до окислення та здатності витримувати високі робочі температури, що робить його придатним для швидкого та рівномірного нагріву в стеці SOFC. Систематично досліджено вплив співвідношення маси порошку до маси куль (1:10 та 1:20) і параметрів розмелу на процес механосинтезу. Встановлено, що підвищення підведення енергії значно прискорює формування фази $MoSi_2$, скорочуючи час реакції приблизно у 1,5 рази. Рентгеноструктурний аналіз підтвердив формування фази $MoSi_2$ з незначною кількістю залишкового молібдену, тоді як кремній виявився рентгеноаморфним, що свідчить про його високу реакційну здатність та структурну розупорядкованість після механічної активації. Для оптимізації параметрів синтезу було проаналізовано передачу енергії під час розмелу та розподіл частинок за розмірами, що забезпечило однорідну морфологію нанопорошку, придатну для подальшої обробки. Синтезований нанопорошок використано для приготування керамічних паст для 3D-друку методом робокастингу (DIW). Реологічні властивості паст було оптимізовано для забезпечення стабільної екструзії та високоточного друку складних геометрій. Ключові параметри друку, включаючи швидкість екструзії, діаметр сопла та швидкість переміщення, було відкориговано для мінімізації дефектів і забезпечення структурної цілісності надрукованих елементів. Після термообробки та спікання надруковані нагрівальні елементи демонстрували швидке та рівномірне підвищення температури, підтверджуючи їх придатність для інтеграції в стеки SOFC та інші високотемпературні системи генерації енергії. У цій роботі запропоновано детальну методологію поєднання механосинтезу та адитивного виробництва для отримання високоефективних керамічних компонентів. Отримані результати сприяють розробці енергоефективних і надійних нагрівальних елементів для передових SOFC та демонструють потенціал матеріалів на основі $MoSi_2$ у високотемпературних енергетичних застосуваннях. Крім того, отримані дані дають уявлення про контроль фазового складу, морфології частинок та параметрів процесу, що є критично важливим для масштабованого виробництва функціональної наноструктурованої кераміки.

1. Introduction

Solid oxide fuel cells (SOFCs) are highly efficient electrochemical devices that directly convert chemical energy stored in gaseous fuels into electrical energy (up to 65%) and high-grade thermal energy (up to 30%). Their advantages include high efficiency, low pollutant emissions, fuel flexibility (ability to operate on hydrogen, synthesis gas, natural gas, biogas, or other hydrocarbons without external reforming), and independence from precious platinum-group metal catalysts [1–2]. The interconnect system and heating elements are key components of SOFC stacks, on the basis of which combined heat and power (CHP) systems are constructed [1].

The material of heating elements, their design, placement within the stack, ability to provide rapid and uniform heating, as well as chemical and mechanical stability under SOFC operating conditions (reducing/oxidizing environment, operating temperatures of 600–800 °C), play a crucial role in ensuring fast system startup and long-term reliability. The startup heating system is designed to uniformly heat the stack to temperatures of ~500–650 °C, at which the fuel cell begins stable electrical power generation.

Traditionally, FeCrAl or NiCr alloys are used; however, they are limited in terms of maximum operating temperature and service life. For high-temperature operation and rapid heating, silicon carbide or $MoSi_2$ (molybdenum disilicide) are employed, as they can withstand more severe heating conditions and provide longer service life. It is well known that $MoSi_2$ exhibits high electrical and thermal conductivity, a high melting point (~2030 °C), and excellent oxidation resistance in air due to the formation of a protective SiO_2 layer on its surface [3–5].

Despite its outstanding properties, obtaining phase-pure $MoSi_2$ remains a challenging technological task. The main difficulties are

associated with the formation of secondary silicide phases such as Mo_5Si_3 and Mo_3Si, which can significantly affect the microstructure and properties of the final material. An additional complication is the existence of two crystalline modifications of $MoSi_2$: a stable high-temperature α-phase and a metastable ß-phase, the formation of which depends on temperature, annealing time, and processing atmosphere. Control of the phase composition is therefore a key factor in achieving the required performance characteristics.

Considering the SOFC stack design, the placement of heating elements to ensure uniform heating of the working zone, as well as the choice of material, remains a relevant technological challenge [6]. When heating elements are located externally, a temperature gradient may arise between the surface and the interior of the stack, slowing down the transition of the entire energy system to operating mode. Alternatively, heating elements can be integrated directly within the SOFC stack, becoming part of the interconnects and providing more uniform and significantly faster heating to the operating temperature (Fig. 1).

Fig. 1. Schematic representation of the SOFC stack design developed at Frantsevich Institute for Problems of Materials Science, NAS of Ukraine, with the possibility of internal heating.

Although internal or built-in heating elements complicate the stack design, the development of additive manufacturing technologies allows for the controlled layer-by-layer deposition (printing) of materials with complex geometry, both in the form of volumetric structures and directly onto surfaces with a high degree of process automation. The robocasting technique, as a form of 3D printing, allows for the production of ceramic materials with complex shapes. Furthermore, the implementation of robocasting using various ceramic pastes with controlled layer thickness and geometry makes it possible to apply coatings onto substrates as well as to produce bulk ceramic components.

Considering the complexity of manufacturing ceramic fuel cell stacks with integrated heating elements, this study focuses primarily on the investigation of the mechanosynthesis of molybdenum disilicide and its application in 3D printing by robocasting for the fabrication of prototype ceramic heaters for SOFC stacks.

Several methods for the synthesis of $MoSi_2$ have been reported in the literature, including solid-state reaction between molybdenum and silicon [7], self-propagating high-temperature synthesis [7–9], mechanical alloying [10–11] followed by heat treatment [12], powder metallurgy techniques (hot pressing [13], spark plasma sintering [14–16]), as well as vapor-phase processes (CVD, PVD) for thin film formation [7, 17]. The solid-state reaction remains one of the most accessible and widely used methods; however, achieving phase purity requires careful control of temperature and processing atmosphere.

Traditional synthesis methods of $MoSi_2$, such as solid-state synthesis or chemical deposition, have several limitations, including the need for high temperatures (above 1400 °C), long processing times, and the risk of forming undesirable secondary phases (Mo_5Si_3, Mo_3Si). This makes it difficult to control the structure and phase composition of the material, which significantly affects its properties.

The use of mechanosynthesis as an alternative route for obtaining $MoSi_2$ is a highly relevant research direction. This method is based on intensive mechanical milling of precursor powders in planetary mills, which enables activation of chemical interactions at the atomic level, reduction of the reaction energy barrier, and formation of the target phase at significantly lower temperatures (600–1000 °C). This approach makes it possible to obtain nanocrystalline or fine-dispersed $MoSi_2$ powders with controlled morphology and homogeneity, which

is important for further application in vacuum sintering, coating deposition, or the fabrication of composite materials.

The study of $MoSi_2$ formation mechanisms during mechanosynthesis is of both practical and fundamental importance for understanding the reactivity of transition metal–silicon systems. Knowledge of phase formation mechanisms, process kinetics, the role of intermediate phases, and the influence of milling parameters enables the development of energy-efficient and environmentally friendly technologies for advanced functional materials.

Thus, investigation of the mechanosynthesis of $MoSi_2$ is relevant from both materials science and applied energy perspectives, as it contributes to the improvement of methods for producing high-temperature materials with optimized properties and reduced energy consumption.

Current achievements, material requirements, processing principles, and prospects for the further development of direct ink writing (DIW) ceramics have been systematically summarized in [18-24]. The feasibility of fabricating mechanically stable ceramic structures using hydrogel-based inks was demonstrated in [23], and a universal self-curable ink formulation suitable for robocasting metals, ceramics, and multi-material components was proposed in [24]. Regarding functional applications, patterned structures produced by DIW have demonstrated controllable Joule heating, although the reported MXene/norepinephrine system represents a conductive composite rather than a conventional sintered ceramics [25]. Regarding 3D printing by direct ink writing (robocasting), a number of studies have been carried out on the fabrication of bulk ceramic materials, including heaters based on molybdenum disilicide [18,19]. Based on experiments with pastes containing 83–85 wt.% $MoSi_2$ powder, prototypes of complex-shaped heating elements were obtained. After heat treatment and sintering, such heaters demonstrated rapid heating. For example, at a power of 1 W, the sample could be heated to approximately 90 °C [18].

The aim of this work is a comprehensive investigation of the development of heating elements for SOFCs, covering the entire technological chain from the synthesis of molybdenum disilicide powders by mechanosynthesis to the fabrication of $MoSi_2$-based heater prototypes using robocasting 3D printing.

2. Experimental

The starting materials were Mo powder (particle size 7–9 μm) and Si powder (particle size 8–10 μm). A mixture of 25 g Mo and 15 g Si was used for the mechanosynthesis process. The mechanosynthesis process was carried out in two stages. At the first stage, to ensure uniform distribution of the components, the mixture was subjected to mixing in a container with stainless steel balls in a planetary mill "Pulverisette-6" under an argon atmosphere using the following regime: powder-to-ball mass ratio (PBR) of 1:10, rotation speed of 150 rpm, and mixing time of 30 min in reverse mode (3 min clockwise and 3 min counterclockwise rotation). At the second stage, the processing conditions were as follows: rotation speed of 400 rpm in continuous mode, argon atmosphere, with powder-to-ball mass ratios of 1:10 and 1:20.

To study the mechano-synthesized powder for the content of Fe entering the material through the friction of stainless steel balls, the powder was subjected to classical chemical analysis using sulfosalicylic acid.

The products obtained after mechanosynthesis were analyzed by X-ray diffraction (XRD) using cobalt radiation. Monitoring of the mechanosynthesis reaction was carried out using an EASY GTM pressure and temperature control system (Fig. 2). The particle size distribution of the synthesized powder was determined by dynamic light scattering (DLS) using a VASCO analyzer. Sintering was performed in a vacuum furnace SPBE-1.3.1/20 (10^{-3} Pa) at a temperature of 1450 °C with a holding time of 1 hour. Annealing was carried out in a vacuum drying oven ("SNVS-4.5.4.5/3.5") with a gradual temperature increase of 50 °C every 30 minutes from 100 °C to 350 °C, followed by a holding time of 1 hour.

For paste preparation, mechanosynthesized $MoSi_2$ powder was used. To obtain a printable paste, an aqueous solution of the PVB binder (9 wt.%) was prepared with the addition of a surfactant in the form of oleic acid (1 wt.%) to prevent particle agglomeration. A homogeneous suspension was obtained by mixing the components for 10 min in an overhead stirrer RIVA OS-20 [18–19].

Subsequently, $MoSi_2$ powder (89 wt.%) was mixed with a PVB binder solution (11 wt.%) using the same overhead stirrer until a homogeneous paste-like mass was obtained. The mixing duration was 5–7 min. To achieve high-quality samples by direct ink writing (DIW),

Fig. 2. EASY GTM pressure and temperature control system.

the paste must meet specific requirements for proper extrusion behavior [20].

The prepared $MoSi_2$–PVB paste exhibited rheological properties suitable for extrusion-based 3D printing. In the shear rate range of 16–43 s^{-1} (nozzle diameter 1.5–2 mm, printing speed 4–8 mm/s), the dynamic viscosity decreased from 7.96 to 4.64 Pa·s, while the fluidity increased from 0.126 to 0.216 $(Pa \cdot s)^{-1}$ [18]. This confirms a pronounced pseudoplastic (shear-thinning) behavior of the paste, which ensures easy extrusion through the nozzle during printing while maintaining shape stability after deposition.

The prepared ceramic paste was loaded into a Tronxy Moore 2 Pro 3D printer (Fig. 3). The printer operates based on the robocasting method, in which the paste is fed from a reservoir by a piston into a screw-driven extrusion system equipped with a nozzle of a specified diameter. During the printing process, parameters such as printing speed, extrusion rate, and nozzle diameter were taken into account [18, 21]. The geometric dimensions of the printed green bodies and sintered heating elements were measured using a digital caliper with an instrumental accuracy of ±0.01 mm.

3. Results and discussion

Figure 4 shows the dependences of pressure and temperature on processing time during the mechanosynthesis of $MoSi_2$ at a rotation speed of 400 rpm with different powder-to-ball mass ratios (PBR) of 1:10 and 1:20. It can be seen that when using a PBR of 1:20, the synthesis reaction is completed in 1 h 46 min, whereas for a PBR of 1:10 it takes 2 h 31 min. Thus, increasing the mechanical load on the powder leads to a reduction in the synthesis time by approximately 1.5 times. This reduction can be

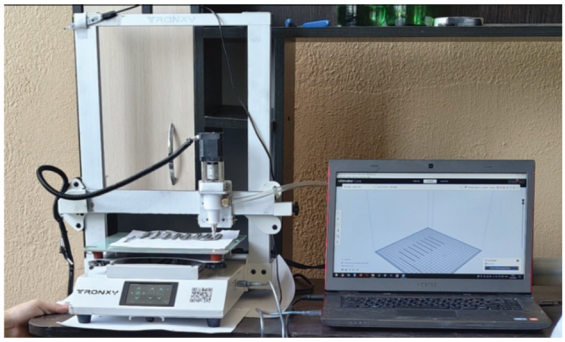

Fig. 3. 3D printer used for fabrication of heating elements.

explained by the higher energy transferred to the powder at a PBR of 1:20 compared to 1:10.

During mechanosynthesis (high-energy ball milling), the powder receives energy as a result of repeated impacts, friction, and shear deformation between the balls and the walls of the milling vessel. The amount of transferred energy directly depends on the mass and number of the balls, rotation speed, and the powder-to-ball ratio. The estimation of the energy transferred to the powder in a planetary ball mill is based on the evaluation of the kinetic energy of the balls and the frequency of their collisions. It should be noted that not all of the balls' kinetic energy is transferred to the powder; therefore, an energy transfer efficiency coefficient is introduced.

The calculated (estimated) mechanical energy load of the system during mechanosynthesis is given below. To estimate the mechanical energy load during mechanosynthesis, the kinetic energy of the ball load was calculated. With a mass of one ball (m_b=0.004 kg), number of balls (N=100), radius of rotation (R=0.08 m) and disk rotation speed (n=400 rpm), the linear velocity of the ball load was approximately (v=3.35 m/s).

1. Ball speed:

$$v = \frac{2\pi Rn}{60} \quad (1)$$

2. Energy of one ball:

$$E_b = \frac{m_b v^2}{2} \quad (2)$$

3. Total kinetic energy of 100 balls:

$$E_\Sigma = NE_b \quad (3)$$

4. Number of revolutions per grinding (processing) time:

$$N_{vol} = n \cdot t \quad (4)$$

5. Total mechanical energy (in a simplified model):

$$E_{mech} = E_\Sigma N_{vol} \quad (5)$$

Table 1. Estimated mechanical energy load of the system during mechanosynthesis.

Powder-to-ball ratio (PBR)	Rotation speed, rpm	Processing time, min	Powder weight, g	Weight of balls, g	Total energy transferred to the powder, kJ
1:10	400	151	40	400	135.3
1:20	400	106	40	800	189.95

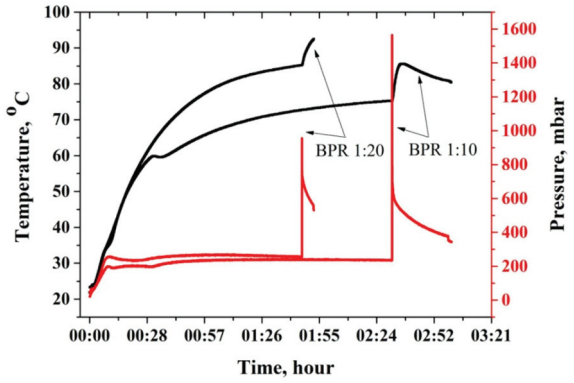

Fig. 4. Temperature and pressure evolution during the mechanosynthesis of $MoSi_2$ at PBR of 1:10 and 1:20.

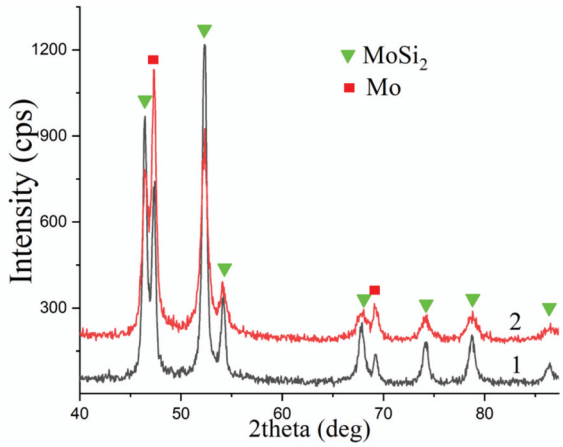

Fig. 5. X-ray diffraction pattern of mechanosynthesized $MoSi_2$ powder: 1 - PBR of 1:10, 2 - PBR of 1:20

Table 1 presents the estimated mechanical energy load of the system during mechanosynthesis under different ball loading conditions.

The values given in Table 1 should be considered as an estimate of the mechanical energy load of the ball–powder system, and not as a directly measured energy absorbed by the powder. Part of the mechanical energy is spent on elastic and plastic deformation of the balls and the walls of the drum, friction, heating and other processes. Therefore, the actual energy transferred to the powder is less than the calculated total mechanical energy. The calculation of 135.3 and 189.95 kJ is an estimate according to a simplified model, and not the strict energy of impacts in the planetary mill. In particular, not all the energy of the balls is transferred with each revolution of the disk.

Phase composition analysis showed that mechanosynthesis leads to the formation of the $MoSi_2$ phase, with the presence of residual Mo. Silicon was not detected in the studied powders by X-ray diffraction analysis; it is assumed that during mechanosynthesis Si becomes X-ray amorphous, which explains its absence in the diffraction patterns.

Figure 5 shows the diffraction patterns of the mechanosynthesized powder obtained at a PBR of 1:10 and the mechanosynthesized powder obtained at a PBR of 1:20. The obtained results showed that increasing the load on the powder, i.e. increasing the ratio of balls to powder by 2 times, did not affect the reduction of the residual free Mo phase (Fig. 5). Increasing the ratio of balls to powder affects only the reduction of the exothermic reaction time. Quantitative X-ray phase analysis showed that at PBR 1:10 (1) less free Mo remains in the material than at PBR 1:20 (2). The powder obtained after mechanosynthesis with PBR 1:10 (1) has the following phase composition: $MoSi_2$ – 85% and Mo – 15%, while at PBR 1:20 (2): $MoSi_2$ – 80% and Mo – 20%.

Since a stainless steel container and balls were used for the mechanosynthesis of $MoSi_2$ powder, after the process was completed, the powder was subjected to an examination of the Fe content. The mechanosynthesized $MoSi_2$ powder obtained using PBR 1:10 had 0.29% Fe in its composition, while at PBR 1:20 it had 0.44% Fe, and after additional homogenization for 1 hour it had 0.47% Fe.

Scanning electron microscopy (SEM) revealed that the $MoSi_2$ powder after mechanosynthesis exhibits a submicron structure with a relatively uniform particle distribution (Fig. 6). The particles are predominantly spherical or semi-spherical in shape, with a rough surface resulting from repeated impacts, friction, and shear deformation in the planetary mill. The use of PBR 1:20 allows obtaining a mechanosynthesized powder consisting of

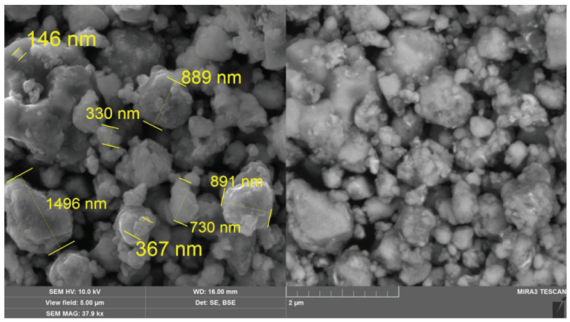

Fig. 6. SEM image of mechanosynthesized $MoSi_2$ powder obtained at PBR of 1:20.

$MoSi_2$ and residual Mo with predominantly submicron particle size (Fig. 6).

Figure 7 presents the results of the particle size distribution analysis of the mechanosynthesized $MoSi_2$ powder obtained by dynamic light scattering (DLS). The graph represents the particle size distribution function, that allows one to evaluate the dispersion, homogeneity, and degree of agglomeration of the powder material. The distribution curve exhibits a predominantly unimodal character with a maximum in the submicron range (approximately 800 nm), indicating the formation of a fine-dispersed powder as a result of high-energy ball milling. This type of distribution confirms the effectiveness of mechanosynthesis not only as a method of $MoSi_2$ phase formation but also as a means of reducing particle size to the submicron level.

The presence of a slight peak broadening or a "tail" in the region of larger particle sizes (1–4 μm) may be attributed to the formation of secondary agglomerates resulting from the high surface energy of particles after mechanical activation. This is a typical phenomenon for mechanosynthesized systems and is associated with processes of cold welding and repeated particle fracture during milling.

Analysis of the distribution parameters D10, D50, and D90, which are 360, 690, and 1370 nm, respectively, allows for a quantitative assessment of powder uniformity. The relatively small interval between D10 and D90 indicates a narrow particle size distribution, which is critically important for:

- stability of the rheological properties of the ceramic paste;
- predictable extrusion behavior during 3D printing by robocasting;
- uniform densification and minimization of porosity during sintering;

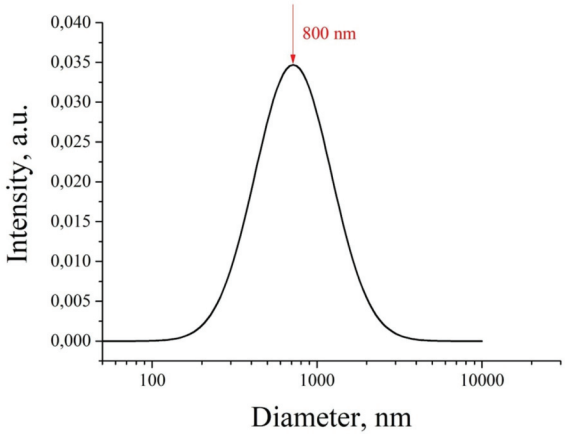

Fig. 7. Particle size distribution of $MoSi_2$ powder after mechanosynthesis (PBR 1:10).

- ensuring homogeneous electrophysical and thermomechanical properties of the final heating elements.

Thus, the obtained particle size distribution confirms the formation of a highly dispersed $MoSi_2$ powder with characteristics suitable for application in additive manufacturing technologies and for the subsequent production of dense high-temperature ceramic components for solid oxide fuel cells.

During the 3D printing experiments using ceramic pastes based on molybdenum disilicide by the robocasting method, it was established that for a nozzle diameter of 1.5–2 mm, the optimal printing speed is in the range of 4–8 mm/s with an extrusion rate of 50–100%, depending on the digital model of the sample (Fig. 8a). Printing was carried out at a temperature of 17–21 °C.

The selection of nozzle diameters (1–2 mm) and printing speeds (4–8 mm/s) was based on experimental optimization of the printability window established in our previous work [18–19]. This nozzle size provides a reliable compromise between preventing nozzle blockages due to powder particle agglomerates and maintaining structural integrity of the printed filaments, with future perspectives of scaling down to 0.6–0.8 mm nozzles as powder homogeneity improves.

Heating elements were deposited onto ceramic plates made of aluminum nitride with dimensions of 32×48 mm. The set layer height was 0.8 mm, the layer width was 1 mm, and the nozzle was positioned 0.25 mm above the zero coordinate. Deposition was performed at a printing speed of 4 mm/s using a nozzle with a diameter of 1 mm. The resulting plate with a deposited $MoSi_2$ heating element is shown in Fig. 8b.

After that, the heating element on the plate was covered with a symmetrical plate measuring 32×48 mm, resulting in a total sample thickness of 4–5 mm. The dimensions of the heating element (cross-section) were 1.5 mm × 4 mm, with a total length of 9 cm.

The obtained samples were then subjected to heat treatment, including annealing and sintering. The sintered plates with deposited heating elements are shown in Fig. 8c. The linear shrinkage and relative density of the sintered components were evaluated in comparison with our previously reported data for DIW-printed ceramic structures [18, 19]. While the initial paste contains 11 wt.% of the PVB binder solution, the solid polymer content accounts for only ~10% of the solution mass, with the volatile solvent evaporating during the drying stage. As a result, the actual mass loss during the debinding and vacuum sintering phases is limited to 1–2%. This leads to a moderate linear shrinkage of approximately 6–10% and a residual porosity of 10–14% in the final sintered parts. Macroscopic inspection confirmed that the sintered heating elements maintained their structural integrity and shape fidelity without critical internal defects, such as severe cracking or interlayer delamination, ensuring the reliability of the conductive pathways.

Now let us consider the current–voltage characteristics of these samples. In publication [19], the current–voltage characteristic of a ceramic heater with a length of 3 cm and a diameter of 4 mm was experimentally obtained and is described by the following equation: $j = 6.5082\ U$. The experimental current–voltage characteristic was obtained at a heater temperature of approximately 90 °C. To estimate the behavior of the element at the operating temperature of ~800 °C, the temperature dependence of the electrical resistivity of $MoSi_2$ was taken into account. According to the known relation $\rho(T) = \rho_0(1 + \alpha(T - T_0))$, the temperature coefficient of resistivity for molybdenum disilicide is approximately $\alpha \approx 2 \times 10^{-3}\ K^{-1}$. With an increase in temperature of ~710 °C, the resistivity of the material increases by approximately 2.4 times.

Thus, the total change in resistance is approximately 15.09 times.

Taking into account both the change in heater geometry and the increase in the electrical resistivity of $MoSi_2$ with temperature up to ~800 °C, the expected current–voltage characteristic of the new sample can be approximated by the following relation: $j \approx 2.58U$.

Fig. 8. $MoSi_2$-based heating element fabricated by DIW: (a) digital model of the sample, (b) heater deposited onto the plate by 3D printing, (c) assembled heating element for SOFC applications.

It should be emphasized that the electrical parameters and *I-V* characteristics presented for the target operating temperature of 800 °C are theoretical estimations. These calculations were extrapolated from experimental data obtained at 90 °C in our previous study [18], taking into account the new geometric parameters of the 3D-printed prototype and the temperature dependence of the electrical resistivity of $MoSi_2$. While this study successfully demonstrates the manufacturing feasibility of the heating elements via 3D printing and sintering, actual experimental validation of the heating performance under real SOFC operating conditions will be the subject of our future investigations.

Thermal analysis indicates that achieving temperatures on the order of 800 °C requires an electrical power of approximately 10–15 W, corresponding to a voltage of about 2 V and a current of 5–6 A for the given heater geometry.

4. Conclusions

A comprehensive approach to the development of heating elements for solid oxide fuel

cell stacks has been developed, including mechanosynthesis of molybdenum disilicide and fabrication of prototypes using robocasting-based 3D printing.

It was established that increasing the powder-to-ball ratio from 1:10 to 1:20 at a rotation speed of 400 rpm leads to an increase in the specific energy transferred to the powder and reduces the synthesis reaction time by approximately 1.5 times. This confirms the decisive role of energy input in the kinetics of $MoSi_2$ phase formation. X-ray diffraction analysis confirmed the formation of the main $MoSi_2$ phase with a small amount of residual molybdenum. Dynamic light scattering analysis showed an average particle size of approximately 800 nm, indicating the formation of a fine-dispersed material suitable for additive manufacturing applications.

A ceramic paste composition based on mechanosynthesized $MoSi_2$ and a PVB binder was developed, exhibiting rheological properties suitable for extrusion-based 3D printing. Optimal printing parameters (nozzle diameter 1–2 mm, printing speed 4–8 mm/s) were determined, ensuring the formation of heating elements with the required geometry.

After heat treatment and vacuum sintering at 1450 °C, functional prototypes of heating elements were obtained, demonstrating stable and rapid heating, which confirms the potential of $MoSi_2$ for the development of integrated heaters in SOFC stacks. The obtained results confirm the effectiveness of combining mechanosynthesis and additive manufacturing technologies for the development of functional high-temperature materials and can be applied in the creation of energy-efficient combined heat and power systems based on solid oxide fuel cells.

Acknowledgements

The authors express their gratitude to the National Academy of Sciences of Ukraine for the support and funding of the research project "Advanced Interconnect System for Ceramic Fuel Cells" (state registration No. 0125U000309).

References

1. Ulf Bossel, Rapid Startup SOFC Modules, Energy Procedia, Volume 28, 2012, Pages 48-56, DOI: 10.1016/j.egypro.2012.08.039.
2. Polishko, I., Ivanchenko, S., Horda, R., ...Lysunenko, N., Kovalenko, L. / Tape casted SOFC based on Ukrainian 8YSZ powder // Materials Today: Proceedings, 2019, 6, pp. 237–241, DOI: 10.1016/j.matpr.2018.10.100.
3. Afiqa Mohamad, Yuji Ohishi, Hiroaki Muta, Ken Kurosaki, Shinsuke Yamanaka. Thermal and Mechanical Properties of α-$MoSi_2$ as a High-Temperature Material. *PSS (Physica status solidi)*, 2018, vol.225, issue 4, 1700448, DOI: 10.1002/pssb.201700448.
4. Bose S., Hecht R. J. Thermal properties of MoSi2 and SiC whisker-reinforced $MoSi_2$. *Journal of materials science*, 1992, vol.27, p. 2749-2752, DOI: 10.1007/BF00540701.
5. Sharif A. A. High-temperature oxidation of $MoSi_2$. *Journal of materials science*, 2010, vol.45, p. 865-870, DOI: 10.1007/s10853-009-4012-8.
6. Serhii Tkachenko, Dmytro Brodnikovskyi, Jan Cizek, Pavel Komarov, Yehor Brodnikovskyi, Yaroslav Tymoshenko, Štefan Csáki, Mykyta Pinchuk, Oleksandr Vasylyev, Ladislav Čelko, Mykola Gadzyra, Tomáš Chráska / Novel Ti–Si–C composites for SOFC interconnect materials: Production optimization // Ceramics International, 2022, 48(19), pp. 27785–27798, DOI: 10.1016/j.ceramint.2022.06.081.
7. Samadzadeh M., Oprea C., Karimi Sharif H., Troczynski T. Comparative studies of the oxidation of $MoSi_2$ based materials: High-temperature oxidation (1000 – 1600 °C). *International Journal of Refractory Metals and Hard Materials*, 2017, vol.69, p. 31-39, DOI: 10.1016/j.ijrmhm.2017.07.015.
8. Yao Z., Stiglich J., Sudarshan T.S. Molybdenum Silicide Based Materials and Their Properties. *Journal of Materials Engineering and Performance*, 1999, vol.8, issue 3, p. 291-304, DOI: 10.1361/105994999770346837.
9. Sang Chul Yeo, Soo Wan Jeon, Jung Eun Lee, Vijay Singh, Sang Hwan Kim. Combustion characteristics of molybdenum–silicon mixtures. *Ceramics International*, 2015, vol.41, issue 1, part B, p. 1711-1723, DOI: 10.1016/j.ceramint.2014.09.113.
10. Ch Gras, D Vrel, E Gaffet, F Bernard. Mechanical activation effect on the self-sustaining combustion reaction in the Mo–Si system. *Journal of Alloys and Compounds*, 2001, vol.314, issue 1-2, p. 240-250, DOI: 10.1016/S0925-8388(00)01221-4.
11. Kesheng Zuo, Shengqi Xi, Jing'en Zhou. Structure evolution and thermodynamics analysis of $MoSi_2$ during mechanical alloying. *Materials Science and Engineering: A*, 2007, vol.445-446, p. 48-53, DOI: 10.1016/j.msea.2006.09.002.
12. Malek Ali, Projjal Basu, Marwa Liwa. Effect of Mo-Si Molar Ratio on the Synthesis of $MoSi_2$

Through Mechanical Alloying. *Synthesis and Reactivity in Inorganic, Metal-Organic, and Nano-Metal Chemistry*, 2013, vol.43, issue 10, p. 1444-1451, DOI: 10.1080/15533174.2012.762783.

13. Peizhong Feng, Akhtar Farid, Xiaohong Wang, Islam S. Humail, Xuanhui Qu. Mechanically activated reactive synthesis of refractory molybdenum and tungsten silicides. *International Journal of Refractory Metals and Hard Materials*, 2008, vol.26, issue 3, p. 173-178, DOI: doi.org/10.1016/j.ijrmhm.2007.05.008.
14. Hao Liang a, Fang Peng, Haihua Chen, Lijie Tan, Qiang Zhang, Cong Fan, Shixue Guan, Xiaolin Ni, Akun Liang , Xiaozhi Yan, Qiwei Hu. High-pressure sintering of bulk $MoSi_2$: Microstructural, physical properties and mechanical behavior. *Materials Science and Engineering: A*, 2018, vol.711, p. 389-396, DOI: 10.1016/j.msea.2017.11.016.
15. Yongxia Li, Wenbo Han, Guiqing Chen, Yehong Cheng, Qiang Yang. Effect of in-situ formed $MoSi_2$ on phase transformation and thermal diffusivity of spark plasma sintered silicon nitride. *Composites Part B: Engineering*, 2017, vol.116, p. 382-387, DOI: 10.1016/j.compositesb.2016.10.080.
16. Hiroyuki Shimizu, Masaru Yoshinaka, Ken Hirota, Osamu Yamaguchi. Fabrication and mechanical properties of monolithic $MoSi_2$ by spark plasma sintering. *Materials Research Bulletin*, 2002, vol.37, issue 9, p. 1557-1563, DOI: 10.1016/S0025-5408(02)00852-8.
17. Gesheva K.A., Ivanova T., Gogova D., Beshkov G. Formation of $MoSi_2$ by rapid thermal annealing in vacuum of CVD – Mo films on silicon substrate. *Vacuum*, 2000, vol.58, issue 1-2, p. 502-508, DOI: 10.1016/S0042-207X(00)00212-8.
18. Naumenko, V.Y., Zyatkevich, D.P., Vedel, D.V. et al. 3D Printing of MoSi2-Based Ceramic Heaters Using the Robocasting Method. P*owder Metall Met Ceram* 63, 343–351 (2024), DOI: 10.1007/s11106-025-00466-4.
19. Naumenko, V.Y., Zyatkevich, D.P., Zgalat-Lozynskyy, O.B. 3D printing technologies using robocasting of ceramic materials based on refractory compounds Mizhvuzivskyi zbirnyk "NAUKOVI NOTATKY", Lutsk, 2024, No78.- c.78-82, DOI: 10.36910/775.24153966.2024.78.11.
20. Derevianko, O.V., Ivanchenko, S.E., Naumenko, V.Y. *et al.* Evolution of Rheological Parameters of Chitosan Hydrogel/Silicon Nitride Paste During 3D Printing by Robocasting for Biomedical Applications. *Powder Metall Met Ceram* 64, 228–242 (2025), DOI: 10.1007/s11106-026-00519-2.
21. Zgalat-Lozynskyy, O.B. Materials and Techniques for 3D Printing in Ukraine (Overview). *Powder Metall Met Ceram* 61, 398–413 (2022), DOI: 10.1007/s11106-023-00327-y
22. Peng, E., Zhang, D., Ding, J. Ceramic Robocasting: Recent Achievements, Potential, and Future Developments. Adv. Mater. 30, 1802404 (2018). DOI: 10.1002/adma.201802404
23. Feilden, E., Blanca, E. G.-T., Giuliani, F., Saiz, E., Vandeperre, L. Robocasting of structural ceramic parts with hydrogel inks, Journal of the European Ceramic Society, Vol. 36, Issue 10, 2525-2533, (2016) DOI: 10.1016/j.jeurceramsoc.2016.03.001.
24. Zhang, D., Jonhson, W., Herng, T. S., Ang, Y. Q., Yang, L., Tan, S. C., Peng, E., He, H., Ding, J. A 3D-printing method of fabrication for metals, ceramics, and multi-materials using a universal self-curable technique for robocasting. *Materials Horizons*. Vol. 7, No. 4. P1083–1090 (2020) DOI:10.1039/C9MH01690B
25. Jiang, P.-Z., Deng, Z., Min, P., et al. Direct ink writing of multifunctional gratings with gel-like MXene/norepinephrine ink for dynamic electromagnetic interference shielding and patterned Joule heating. Nano Research. Vol. 17, P. 1585–1594, (2024) DOI: 10.1007/s12274-023-6044-9